Mars-Ward Ion Flows in the Martian Magnetotail: Mars Express Observations

Chi Zhang, Yoshifumi Futaana, Hans Nilsson, Zhaojin Rong, Moa Persson, Lucy Klinger, Xiaodong Wang, Gabriella Stenberg Wieser, Stas Barabash, Chuanfei Dong, et al.

Geophysical Research Letters

RESEARCH LETTER
10.1029/2022GL100691

Mars-Ward Ion Flows in the Martian Magnetotail: Mars Express Observations

Chi Zhang[1,2,3], Yoshifumi Futaana[3], Hans Nilsson[3], Zhaojin Rong[1,2], Moa Persson[4,5], Lucy Klinger[6], Xiaodong Wang[3], Gabriella Stenberg Wieser[3], Stas Barabash[3], Chuanfei Dong[7], Mats Holmström[3], Yasir Soobiah[8], and Yong Wei[1,2]

[1]Key Laboratory of Earth and Planetary Physics, Institute of Geology and Geophysics, Chinese Academy of Sciences, Beijing, China, [2]College of Earth and Planetary Sciences, University of Chinese Academy of Sciences, Beijing, China, [3]Swedish Institute of Space Physics, Kiruna, Sweden, [4]IRAP, CNRS-UPS-CNES, Toulouse, France, [5]Now at Graduate School of Frontier Sciences, The University of Tokyo, Kashiwa, Japan, [6]Beijing International Center for Mathematical Research, Peking University, Beijing, China, [7]Princeton Plasma Physics Laboratory and Department of Astrophysical Sciences, Princeton University, Princeton, NJ, USA, [8]Solar System Exploration Division, NASA Goddard Space Flight Center, Greenbelt, MD, USA

Abstract We investigate Mars-ward planetary ions (O^+ and O_2^+) in the Martian magnetotail that potentially reduce the amount of escaping ions. The global properties of Mars-ward flows in the Martian magnetotail are characterized, based on over 13-years of ion data (May 2007–December 2020) collected by the Analyzer of Space Plasma and Energetic Atoms instrument on Mars Express. We find that Mars-ward flows are frequently observed in the vicinity of the crustal fields, implying that crustal fields may play a key role in producing such flows. The occurrence rate and sunward flux are found higher during solar maximum than solar minimum. However, the occurrence rate and flux of Mars-ward flows are relatively low. This is different from the case at Venus, where the planetward flows can significantly decrease the total escape rates of ions.

Plain Language Summary Without the protection of an intrinsic magnetic field, solar wind can interact directly with the Martian atmosphere and drive ion escape, which plays a vital role in the evolution of the planetary atmosphere. It was shown that, on average, all Martian ions accelerated by the solar wind flow downstream and escape to interplanetary space. However, some planetary ions can flow sunward or Mars-ward in the tail, possibly reducing total ion escape. The mechanism and role of these Mars-ward ions remain unclear. Here, we present a statistical analysis that reveals the global properties of Mars-ward flows at Mars based on over 13 years of Mars Express data. Our results suggest that crustal fields may play a role in driving Mars-ward flows. We also show that Mars-ward flows might have negligible influence on total ion escape at Mars regardless of solar activity level. This finding can help us understand ion escape and tail dynamics at Mars.

Key Points:

- Mars-ward ion flows in the magnetotail occur more frequently and with a higher flow flux during solar maximum
- The occurrence rate and flux of planetward flows at Martian magnetotail are relatively lower than the case at Venusian magnetotail
- A strong correlation between crustal fields and Mars-ward flows is identified

Correspondence to:
C. Zhang,
zhangchi@mail.iggcas.ac.cn

Citation:
Zhang, C., Futaana, Y., Nilsson, H., Rong, Z., Persson, M., Klinger, L., et al. (2022). Mars-ward ion flows in the Martian magnetotail: Mars Express observations. *Geophysical Research Letters*, *49*, e2022GL100691. https://doi.org/10.1029/2022GL100691

Received 9 AUG 2022
Accepted 13 OCT 2022

Author Contributions:
Data curation: Yoshifumi Futaana, Hans Nilsson, Moa Persson, Stas Barabash, Mats Holmström
Formal analysis: Chi Zhang, Hans Nilsson
Funding acquisition: Zhaojin Rong, Yong Wei
Investigation: Chi Zhang, Zhaojin Rong, Xiaodong Wang, Gabriella Stenberg Wieser
Methodology: Chi Zhang
Project Administration: Yoshifumi Futaana, Stas Barabash, Mats Holmström
Software: Chi Zhang
Supervision: Yoshifumi Futaana, Zhaojin Rong, Yong Wei
Validation: Yoshifumi Futaana, Hans Nilsson, Zhaojin Rong, Moa Persson, Xiaodong Wang, Gabriella Stenberg Wieser, Stas Barabash, Chuanfei Dong, Yasir Soobiah
Visualization: Chi Zhang
Writing – original draft: Chi Zhang
Writing – review & editing: Yoshifumi Futaana, Hans Nilsson, Zhaojin Rong, Moa Persson, Lucy Klinger

1. Introduction

It is widely accepted that solar wind interaction with Mars is a critical factor in atmosphere removal (e.g., C. Dong, Lee, et al., 2018; Jakosky et al., 2018). The lack of global intrinsic magnetic fields allows solar wind to directly interact with the Martian atmosphere and scavenge the planetary ions to escape away (e.g., Barabash et al., 2007; C. Dong et al., 2014, 2015; C. Dong, Bougher, et al., 2018; Y. Dong et al., 2015; Lundin et al., 1989). As it approaches Mars, the solar wind flow, which carries a "frozen-in" interplanetary magnetic field (IMF), will be decelerated and deflected upon interaction with the Martian ionosphere, resulting in an induced magnetosphere (e.g., Luhmann et al., 2004; Y. Ma et al., 2002; C. Zhang et al., 2022). Correspondingly, the solar wind accelerates planetary ions via the electromagnetic forces, such as motional electric fields (Barabash et al., 1991; C. Dong et al., 2014; Fang et al., 2008), Hall electric fields (Dubinin et al., 2011; Lundin, 2011), and ambipolar electric fields (e.g., Collinson et al., 2019; Y. J. Ma et al., 2019; Xu et al., 2021). In addition, localized intense crustal fields complexify the Martian magnetosphere and affect ion escape (e.g., Connerney et al., 2005; C. Dong et al., 2015; Y. Dong et al., 2015; Fang et al., 2010; Ramstad et al., 2016; C. Zhang et al., 2021).

The motion of Martian ions show that they are accelerated by solar wind, and on average, will flow downstream or tailward and eventually escape into interplanetary space (Dubinin et al., 2018; Fränz et al., 2015; Nilsson et al., 2012). Nonetheless, not all planetary ions flow downstream.

For Venus, which also possesses an induced magnetosphere owing to the interaction between solar wind and its ionosphere, previous studies have reported on the presence of Venus-ward ions in the induced magnetotail, which probably reduce ion escape (e.g., Dubinin et al., 2012, 2013; Kollmann et al., 2016; Lundin, 2011; Persson et al., 2018, 2020). In these studies, these flows are also referred to as "return flows." Furthermore, Kollmann et al. (2016), Persson et al. (2018), and Masunaga et al. (2019) found that the occurrence rate of Venus-ward flows and the total Venus-ward flux at Venusian tail seems to increase from solar minimum to solar maximum, leading to a decrease in the total net escape rate of heavy ions at solar maximum. This indicates that Venus-ward flows can significantly impact the ion escape at Venus and its atmospheric evolution (Persson et al., 2020).

It is expected that similar physics could also occur at Mars. The Mars-ward ions were also present in the Martian tail current sheet, and they can be explained by magnetic reconnection (Harada et al., 2015a, 2015b, 2017, 2020). However, these studies only concern the Mars-ward flux or flow in the current sheet. Therefore, the global properties of Mars-ward flows in the Martian magnetotail are still not completely understood. The key question is whether Mars-ward flows significantly reduce ion escape at Mars as they do at Venus. The relationship between Mars-ward flows, solar wind conditions, and crustal fields are still unclear. Targeting these problems, we utilize 13 years of ions observations made by Mars Express (MEX) to reveal the global properties of Mars-ward flows, their effects on ion escape, their variation in the solar cycle, and their comparison to Venusian return flows. Studying these flows is beneficial to understanding the tail dynamics and the evolution of the Martian atmosphere.

2. Data Sets and Coordinates

In this study, we used 13 years of ion observations (May 2007–December 2020) made by the Ion Mass Analyzer (IMA), which is part of the Analyzer of Space Plasma and Energetic Atoms (ASPERA-3) instrument package on Mars Express (MEX) (Barabash et al., 2006). By stepping the deflection voltage for 16 steps in the entrance deflection system, IMA measured ions with the field of view (FOV) of $90^{\circ} \times 360^{\circ}$. IMA steps the deflection voltage for 16 steps in the entrance deflection system to cover the elevation to $\pm 45°$ with a resolution of 5.6°. IMA measures 96 different energy-per-charge (E/q) levels in 12s. By combination of elevation scan and energy scan, IMA provides a full 3-D ion velocity distribution function with a cadence of 192s (16 steps × 12s). Before May 2007, the energy range was 30 eV/q–32 keV/q. From May 2007 to November 2009, the range was 10 eV/q–25 keV/q. After November 2009, the energy range was 1 eV/q–15 keV/q. IMA can determine the mass of ions using a magnetic system. Finally, we can obtain a full ion distribution in 192s that consists of 32 mass channels × 96 energy steps × 16 azimuthal directions × 16 elevation directions. However, note that the elevation sweeps are off for low-energy ions with E/q < 50 eV/q, leads to a narrow FOV and incomplete measurements for the low-energy ions (Barabash et al., 2006).

In this study, we use Mars Solar Orbital (MSO) coordinates, where $\overrightarrow{X}_{\mathrm{MSO}}$ points from Mars to the Sun, $\overrightarrow{Y}_{\mathrm{MSO}}$ points opposite to Mars' orbital velocity, and $\overrightarrow{Z}_{\mathrm{MSO}}$ completes the right-handed system.

3. Method

3.1. Moment Calculation

To study the Mars-ward flows, we mainly use moment data based on the 3D velocity distribution of ions. It is necessary to remove the noise before the moment calculation, the first of which is the "proton ghost" or also called as "spill-over protons" (Fedorov et al., 2011; Fränz et al., 2006). Part of the H^+ deflected by the magnetic field of the mass determination will hit the surface of magnets and subsequently scatter and cause a signal on a broad range of mass channels, which can affect the moment calculation for heavy ions. In addition, solar ultraviolet (UV), and the Mars Advanced Radar for Subsurface and Ionosphere Sounding (MARSIS) which was onboard the Mars Express also affect ion measurements (Voshchepynets et al., 2018). In this study, we have removed all known types these noise contaminations by following the same method as in Nilsson et al. (2010, 2011, 2012, 2021).

After this, we apply the multispecies fitting technique to separate the distribution of different species (e.g., H^+, He^{2+}, O^+, and $O_2{}^+$). This method, based on fitting a Gaussian distribution function for each species, was discussed and successfully applied for IMA data (Rojas-Castillo et al., 2018).

Each ion detected by IMA can be represented in a distribution function in phase space, $f\left(\vec{V}\right)$, where $\vec{V} = (V_x, V_y, V_z)$ represents the particle's velocity. $f\left(\vec{V}\right)$ can be written in terms of the measured differential particle flux and energy:

$$f\left(\vec{V}\right) = \frac{m^2}{2E} J(E, \Omega) \tag{1}$$

where m is the particle's mass, E is particle's energy, and the differential number flux (J) is a function of energy and the solid angle Ω (e.g., Fränz et al., 2006). We can then calculate the density and velocity through the plasma moments, defined as:

$$M^k = \int f\left(\vec{V}\right) \vec{V}^k d\vec{V} \tag{2}$$

Therefore, the density, 0th moment ($k = 0$) can be written as:

$$n = \int f\left(\vec{V}\right) d\vec{V} \tag{3}$$

In the spherical coordinates of IMA, it can be rewritten as:

$$n = \int d\varphi \int \cos(\theta) d\theta \int v^2 f\, dv \tag{4}$$

where θ, φ are the elevation and azimuth angles, respectively. The elevation angle corresponds to an angle between the particle's velocity and XY_{IMA} plane (see Figure 1 of Futaana et al. (2021)); for example, $\theta = 90(-90)^\circ$ is the $+\vec{Z}_{\mathrm{IMA}}$ ($-\vec{Z}_{\mathrm{IMA}}$), while $\theta = 0^\circ$ represents the XY_{IMA} plane. The azimuth angle φ is in the XY_{IMA} plane, opening from $+\vec{X}_{\mathrm{IMA}}$ with a positive right-hand rotation at $+\vec{Z}_{\mathrm{IMA}}$. V represents the ion's speed, calculated by $V = \sqrt{2E/m}$.

Similarly, we can find the flux of each direction from 1st moment:

$$\begin{aligned} F_x = nV_x &= \int \cos(\varphi) d\varphi \int \cos^2(\theta) d\theta \int v^3 f\, dv \\ F_y = nV_y &= \int \sin(\varphi) d\varphi \int \cos^2(\theta) d\theta \int v^3 f\, dv \\ F_z = nV_z &= \int d\varphi \int \cos(\theta)\sin(\theta) d\theta \int v^3 f\, dv \end{aligned} \tag{5}$$

Therefore, the velocity of particles in IMA frame can be obtained:

$$\vec{V} = (V_x\hat{x}, V_y\hat{y}, V_z\hat{z}) = \left(\frac{F_x\hat{x}, F_y\hat{y}, F_z\hat{z}}{n}\right) \tag{6}$$

Finally, we convert the velocity into an MSO frame and correct the spacecraft velocity.

In order to obtain a reliable velocity, we calculate moments based on ions with energy-per-charge higher than 50 eV/q. The first reason is that the incomplete ion measurement of low-energy ions would affect the moment calculation. The second reason is that low-energy ions (E/q < 50 eV/q) might be influenced by spacecraft potential. Both the energy and the viewing direction will be changed and distorted when the ion energy is less than twice the spacecraft potential (Bergman et al., 2020). The typical potential of MEX is lower than 10 V (Fränz et al., 2006), which indicates that our moment data of ions with an E/q > 50 eV/q is reliable. Using measurements

above 50 eV/q results in moments that are incomplete in energy, but in a well-defined and predictable manner. A similar study using the lower energy (E/q < 50 eV/q) data is reserved for a further study.

3.2. Selecting Criteria of the Mars-Ward Flows

We set the following selection criteria to find the sunward flows events:

1. The spatial region we survey is the magnetotail, that is, $X_{MSO} < 0$ and $R_{MSO} = \sqrt{Y_{MSO}^2 + Z_{MSO}^2} < R_{MPB}$, where ($X_{MSO}$, Y_{MSO}, Z_{MSO}) represent the position of MEX. R_{MPB} represents the time-averaged radial position of the magnetic pile-up boundary (MPB) from the model of Trotignon et al. (2006).
2. To guarantee that the ions are well resolved by IMA, particularly in the Sun and tail direction (which are important for evaluating the Mars-ward flows), we only include the data when the elevation angle of the Sun and anti-Sun directions are within the FOV of IMA frame, meaning $|\theta_{Sun}| < 45^{\circ}$, $|\theta_{anti-Sun}| < 45^{\circ}$, where $\theta_{Sun}(\theta_{anti-Sun})$ represents the elevation angle of Sunward (anti-Sunward) direction in IMA frame. This step helps us at least to obtain a reliable estimate of the V_x component of ions.
3. We only do the moment calculation for the full distributions which are not seriously contaminated by noise (the number of removed counts is less than half of the number of total counts). After noise removal, we require that the number of total counts of high-energy ions (E/q > 50 eV/q) for each full distribution is larger than 10, to ensure the moment calculation is statistically viable.
4. By following Kollmann et al. (2016) and Harada et al. (2015b), we select the Mars-ward flow events, which satisfy that the bulk velocity of O^+ or O_2^+ is sunward, that is, $V_x > 0$. This assumes that the Mars-ward flow is identical to the sunward flow, which is basically feasible in the magnetotail.
5. Due to the spacecraft blockage in the FOV of the IMA, we have to visually inspect the events and excluded the events which the sun-direction, anti-sun direction, or the main population of ions were blocked by spacecraft.

4. Case Study

Figure 1 shows an overview of a typical Mars-ward flow event that occurred during 06:55–07:15 on 11 February 2016. Figures 1a and 1b show the trajectory of MEX projected onto the XR_{MSO} plane and the YZ_{MSO} plane (red line), where $R_{MSO} = \sqrt{(Y_{MSO}^2 + Z_{MSO}^2)}$. As shown in the energy-time spectrogram of electrons (Figure 1c), MEX crossed the magnetic pile-up boundary (MPB) and entered the magnetosphere at ~06:58 (see the black vertical line in Figure 1), characterized by in the disappearance of the heated electrons (Figure 1c). After about 30 min, MEX crossed the outbound MPB at 07:22 (not shown here).

This event occurred during 07:02:56–07:06:08, when MEX was located at (−0.8, 0.77, 0.15) Rm (Rm = 3396 km, Mars radius) with an altitude of 395 km (see the red-shaded region in Figures 1c–1h), which was within the Martian magnetotail. During this period, MEX measured heated heavy ions (Figures 1d and 1e) with an energy range from 10 eV/q to 200 eV/q. The bulk velocity of both O^+ and O_2^+ were Mars-ward (Figure 1g), implying that they were returning toward Mars.

We plotted the angular distribution of O+, O_2^+ in IMA frame to check the reliability of the bulk velocity and studied the ions' motion in more detail (see Figures 1h and 1i). The shaded region is the FOV of the IMA during this event. We found that the main populations of O^+ and O_2^+ are within the FOV, implying that the ion distribution was resolved. Therefore, this event meets all criteria in Section 3.2 and can be regarded as a Mars-ward flow event.

Of particular interest here is that this event occurred around crustal fields, which have enhanced magnetic field strength, as calculated by the Martian crustal fields model (Figure 1g) (Gao, Rong, Klinger, et al., 2021). This suggests that crustal fields might play a key role in driving Mars-ward flow.

For this event, the net sunward flux of O^+ and O_2^+ is about 6.4×10^5 and 4.8×10^5 $cm^{-2}s^{-1}$ respectively, which is about one order of magnitude lower than the average observed escape flux in the magnetotail (on the order of 10^6 $cm^{-2}s^{-1}$) (e.g., Brain et al., 2015; Inui et al., 2019; Nilsson et al., 2011, 2021).

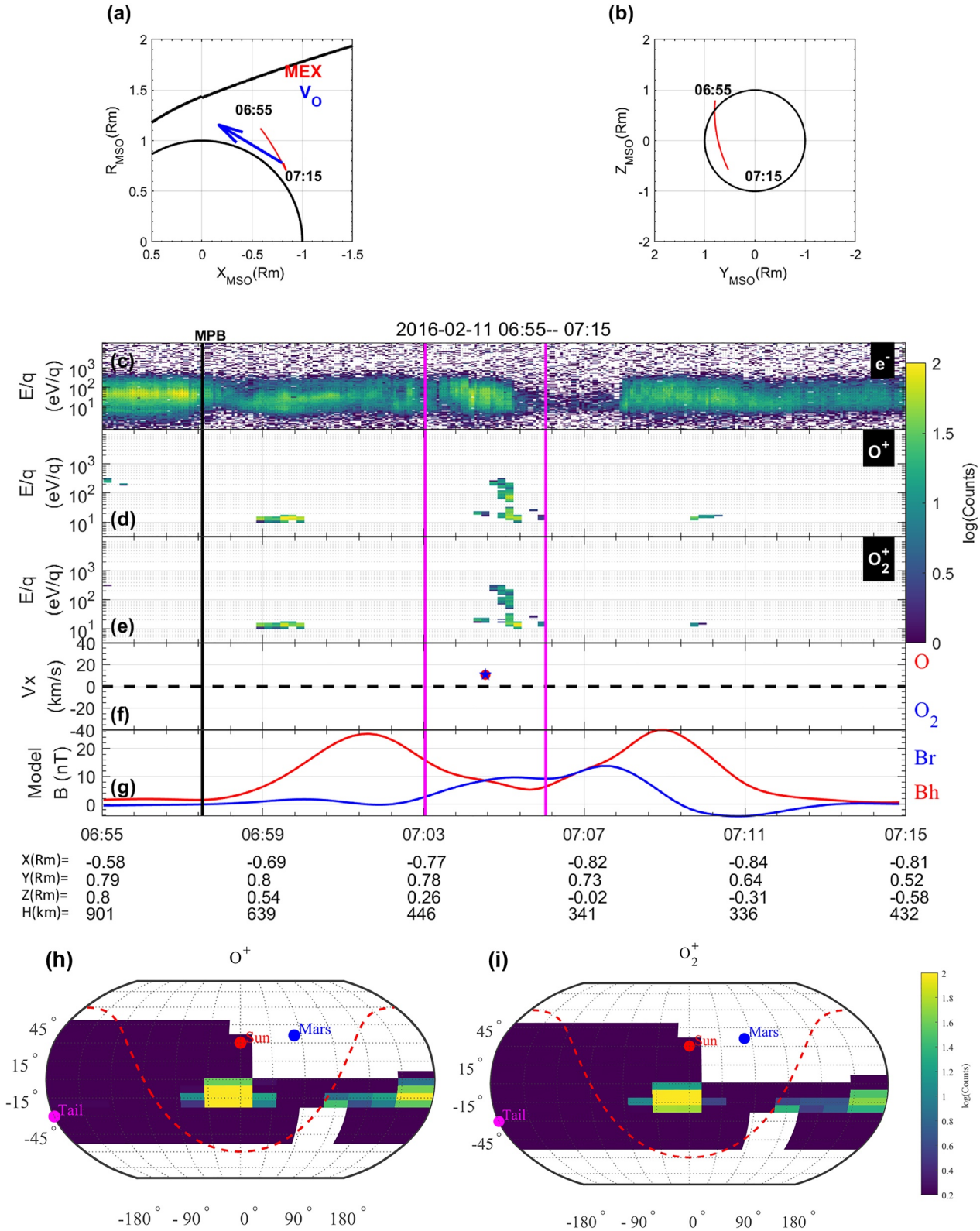

Figure 1.

5. Statistical Results

To draw a global picture that surveys the properties of Martian Mars-ward flows, we conducted a statistical analysis of Mars-ward flow events based on over 13 years of IMA data, measured from May 2007 to December 2020. We found 98 events of sunward O^+ and 134 events of sunward O_2^+ based on the criteria listed in Section 3.2. The period of each event was less than 6 min, and only one data point of bulk velocity that corresponded to each event could be derived. Note that Mars-ward flows are different from the nightside heavy ions precipitations studied by Diéval et al. (2013) and Hara et al. (2018), in which only the Mars-ward flux in low-altitude ionosphere (<350 km) was considered.

5.1. Spatial Distribution in MSO Frame

Figures 2a and 2b show maps of the total number of data points with a determined bulk velocity of O^+ and O_2^+, respectively in each bin with a size of 0.2 Rm × 0.2 Rm. A single data point corresponds to a full distribution. The majority of the data for both O^+ and O_2^+ is located in the terminator region, which is due to a bias in the IMA attitude. Because we require that the IMA can measure both sunward ions and anti-sunward ions (see Section 3.2), which is more probable in the terminator region. Still, we have significant coverage of the entire tail up to 2.5 Rm downstream from the tail.

We project the bulk velocity for 98 events of Mars-ward O^+ and 134 events of Mars-ward O_2^+ respectively onto the XR_{MSO} plane (Figures 2c and 2d). Figures 2e and 2f show the spatial occurrence rate of Mars-ward O^+ and O_2^+, respectively. This rate is calculated by $\frac{N_{events}}{N_{total}}$, where N_{events} represents the total Mars-ward events and N_{total} the total number of data points in each spatial bin. The gaps or white region represent zero Mars-ward flow events in that bin. Clearly, the spatial occurrence rate is higher near Mars ($R_{MSO} < 0.5$ Rm and $X_{MSO} > -1.5$ Rm), whereas Mars-ward flows disappear beyond $X_{MSO} < -2$ Rm. Furthermore, the spatial occurrence rate is generally very low, with the largest value of 0.13 (Figures 2e and 2f).

5.2. Influence of Crustal Fields

In the case study discussed in Section 4, Mars-ward flows occurred above the crustal fields, which might indicate that the flows are associated with crustal fields. Here, we survey the spatial distribution of Mars-ward flow events in geographic coordinates to investigate the possible correlation with crustal fields.

Figures 3a and 3b map the total number of data points with a determined bulk velocity of O^+ and O_2^+ in each bin with a size of 20° × 20° in geographic coordinates. There are more observations near the equator region due to the bias of orbit coverage and the IMA's attitude. Figures 3c and 3d show the location of events of Mars-ward O^+ and O_2^+ in geographic coordinates that overlap with crustal fields at 160 km, which was obtained from a crustal fields model (Gao, Rong, Klinger, et al., 2021), respectively. Figures 3c–3f shows that most events for both O^+ and O_2^+ occurred above magnetic anomalies, especially in the strongest crustal fields region (Latitude ∼ −50, Longitude ∼ 180).

Figures 3g and 3h shows in greater detail the dependence between the occurrence rate of Mars-ward flows and the crustal fields' strength. Calculating the strength for each data point using the model of Gao, Rong, Klinger, et al. (2021), we find a clear correlation between crustal field strength and Mars-ward O^+ and O_2^+. In the rightmost bin (80–90 nT), the likelihood of Mars-ward flow is nearly 2–3 times the planetary average (0.0077 and 0.0107 for O^+ and O_2^+).

These results suggest that crustal fields might play a key role in driving Mars-ward flows. We also surveyed the relationship between these flows and the elevation angle of the crustal fields, but found no clear dependence

Figure 1. Overview of the typical Mars-ward flow events that occurred during 06:55–07:15 on 11 February 2016. (a, b) Mars Express orbital trajectory during this event (red lines). Views are shown (a) in the XR plane and (b) in the YZ plane. The black curves in panel (a) denote the magnetic pile-up boundary (MPB) using the model in Trotignon et al. (2006). The blue arrow is the bulk velocity direction of Mars-ward O^+. The energy spectrum of electrons is shown in panel (c), for O^+ in panel (d), and O_2^+ in panel (e). (f) Shows the V_x of O^+ and O_2^+. (g) Shows the horizontal (red line) and radial (blue line) magnetic fields calculated by the crustal fields model (Gao, Rong, Klinger, et al., 2021). (h, i) Display the angular distribution of O^+ and O_2^+ in the Ion Mass Analyzer frame, respectively. The red dashed lines in panels (h and i) represent the boundary that separates sunward and tailward direction. Note that the angular direction in panels (h and i) is the flow direction of ions. The black vertical line denotes the crossing of MPB. The magenta vertical lines in panels (c–g) represent the interval of Mars-ward flow event.

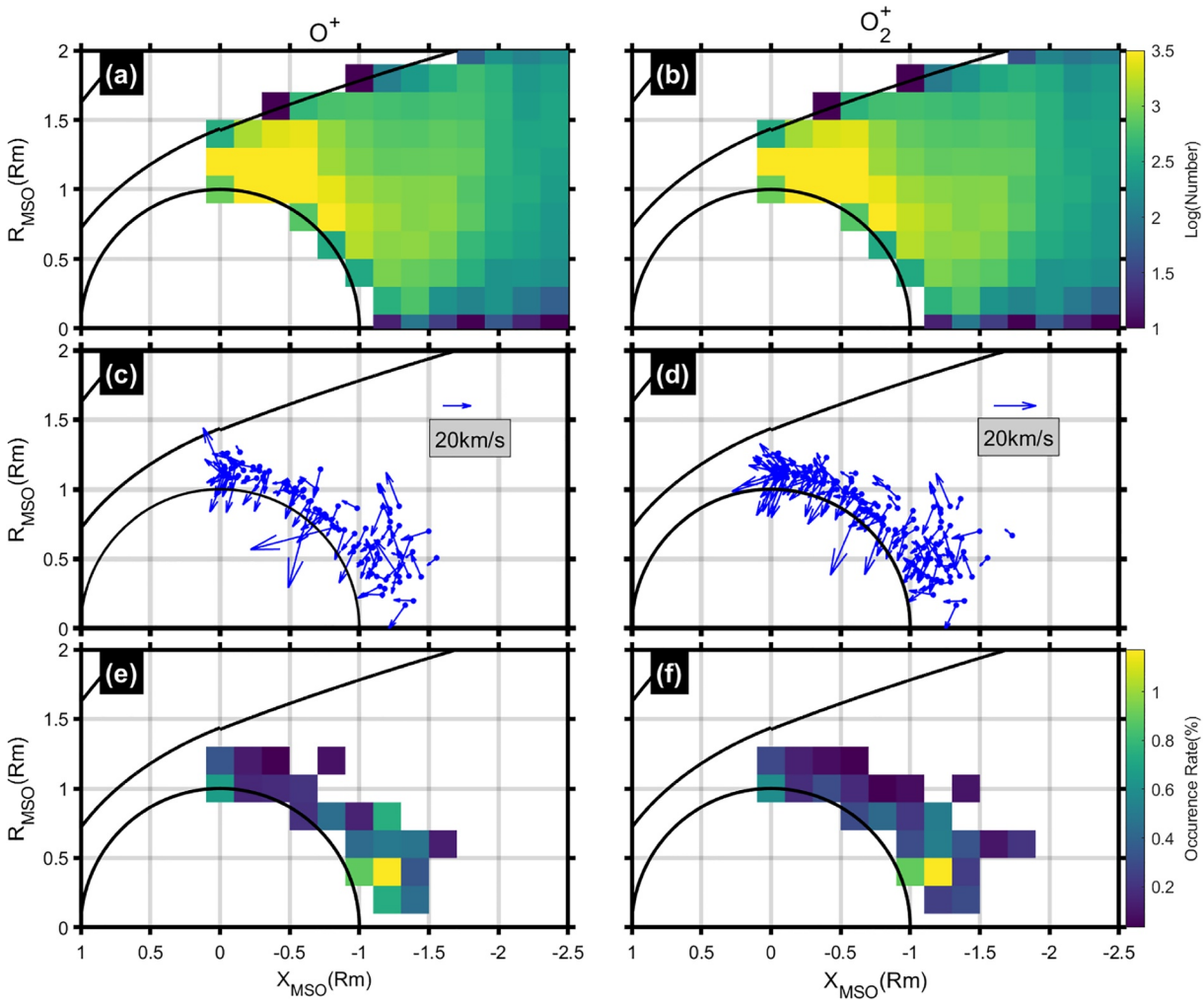

Figure 2. (a, b) Show the total number of the data points with determined bulk velocity of O^+ and O_2^+ in XR_{MSO} plane. (c, d) Display the projection of the bulk velocity of 98 events of Mars-ward O^+ and 134 events of Mars-ward O_2^+, respectively. (e, f) Show the spatial occurrence rate of Mars-ward O^+ and O_2^+, respectively. In all panels, black lines indicate the magnetic pile-up boundary, as found in the model of Trotignon et al. (2006), while black half-circles represent Mars.

(details not shown here). However, the low time resolution (192 s) of the IMA cannot resolve the fine structures of magnetic anomalies, which might affect this result.

5.3. Influence of Solar Activity Level

Kollmann et al. (2016) found that there is a correlation between Venus-ward flows and solar activity level. Our data set covers over 13 years, corresponding to more than one solar cycle (one solar minimum to the next solar minimum), which provides an opportunity to investigate the relationship between Mars-ward flows and solar activity level at Mars.

Based on the variations of the F10.7 index as shown in Figure 4a, we divide the data into three segments, which correspond to two solar minimum periods (green regions) and one solar maximum period (yellow region). Note that our results will not significantly be affected although the F10.7 index is measured at Earth.

From Figure 4b, we see that the temporal occurrence rate of both Mars-ward O^+ and O_2^+ is higher during solar maximum, indicating a correlation with solar activity level. This is similar to the case at Venus and implies that Mars-ward flows might become more significant during solar maximum. However, the low temporal occurrence rate (on the order of 10^{-3} or 10^{-4}) indicates they do not dominate on Mars, regardless of the solar activity level,

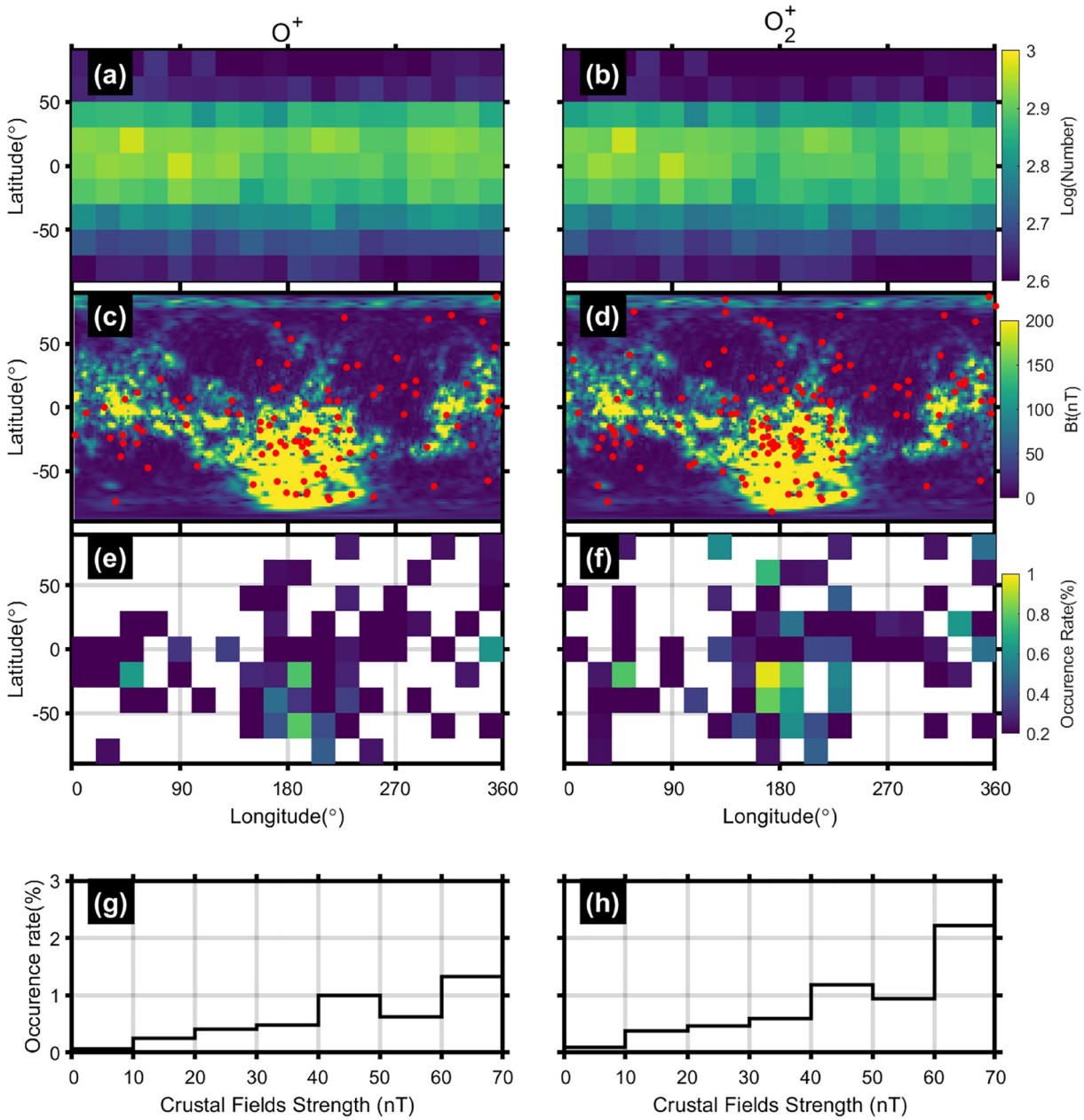

Figure 3. (a, b) Show the map of total number of data points with determined bulk velocity of O^+ and O_2^+, respectively in geographic coordinates. (c, d) Display the locations of 98 events of Mars-ward O^+ and 134 events of Mars-ward O_2^+, respectively, which are represented by red dots overlapping a crustal fields model (Gao, Rong, Klinger, et al., 2021). (e, f) Show the spatial occurrence rate of Mars-ward O^+ and O_2^+, respectively. (g, h) Show the occurrence rate of Mars-ward flows versus crustal magnetic fields strength, respectively.

while for Venus they can reach an occurrence rate as high as 0.8 (Kollmann et al., 2016). However, we have to remind the readers that we ignore the low-energy ions (E/q < 50 eV/q). We will discuss it in the following section.

To obtain the global response of sunward and tailward flux and its dependence on the solar activity level, we follow Nilsson et al. (2010) and Ramstad et al. (2015, 2018) to reconstruct the average ion distributions in the MSO frame for the period of each segment, where we re-binned the data into an average ion distribution by using an angular discretization step of $22.5^\circ \times 22.5^\circ$ and an energy table that is the same as the post-2009 IMA one (1 eV/q–15 keV/q). The averaged ion distributions are averaged over the spatial region within $X_{MSO} < -1$Rm and $R < 1.5$ Rm, which is within the nominal magnetotail. Note that the low-energy ions (<50 eV/q) are also excluded in the averaged distributions due to uncorrected spacecraft potential.

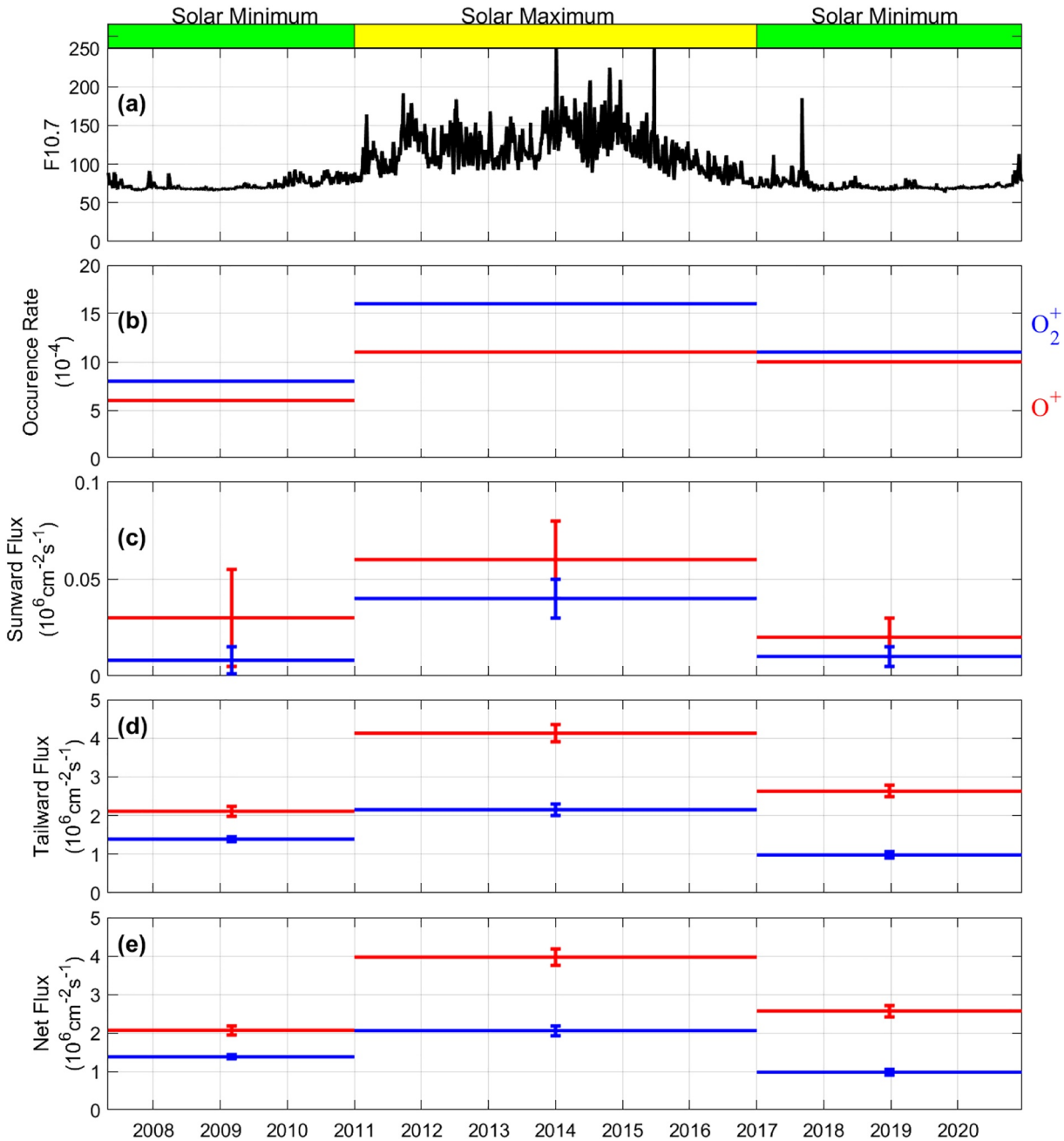

Figure 4. (a) F10.7 index; (b) temporal occurrence rate of Mars-ward O^+ (red) and O_2^+ (blue); (c–e) show the sunward, tailward, and net flux of O^+ and O_2^+, respectively. The green (yellow) shadow regions above this figure represent the time interval of solar minimum (solar maximum). The lengths of the error bars in panels (c–e) are $2 \times \frac{1.96\sigma}{\sqrt{n}}$, representing a 95% confidence interval, where is the $\frac{\sigma}{\sqrt{n}}$ is the standard error of the mean.

Based on the averaged ion distribution for the period of each segment, we can calculate the sunward (or Mars-ward) flux, the tailward flux and the net flux for both O^+ and O_2^+ (Figures 4c–4e). Figures 4c and 4d show that the sunward flux is approximately two orders of magnitude lower than the tailward flux for the whole time, suggesting that tailward-escaping ions were dominating regardless of solar activity level. Furthermore, although the sunward flux reaches higher levels during solar maximum (Figure 4c), the more enhanced tailward flux (Figure 4d) leads to an increased net escape of ions (Figure 4e), which is different to the case at Venus where the net escape is reduced during solar maximum. Our results are also consistent with previous studies that positively

correlate net escape and solar activity level at Mars (e.g., Y. Dong et al., 2017; Dubinin et al., 2017; Nilsson et al., 2021; Ramstad et al., 2015).

6. Discussion and Conclusion

Using over 13 years of ion data that was measured by the IMA onboard Mars Express, we performed a statistical survey on Mars-ward flows of heavy ions above 50 eV/q (O^+ and O_2^+) in the Martian magnetotail. Our study provides a global picture of such Mars-ward flows, which could help us understand plasma dynamics and ion escape at Mars. The main results can be summarized as follows:

1. Both the Mars-ward O^+ and O_2^+ mainly occur around crustal fields and are associated with strong crustal fields, indicating that they might play a key role in generating Mars-ward flows.
2. During solar maximum, as opposed to solar minimum, the temporal occurrence rate of Mars-ward flows increases and the sunward flux is higher. However, more enhanced tailward flux still leads to greater ion removal during solar maximum.
3. The temporal occurrence rate of Mars-ward flows (on the order of 10^{-3}–10^{-4}) are low regardless of solar activity level. Furthermore, the sunward flux above 50 eV/q is about two orders of magnitude lower than the tailward flux, indicating that most of the high-energy ions were escaping to interplanetary space rather than returning to Mars. This result suggests that Mars-ward flows might not reduce the ion escape significantly at Mars during any solar activities, which is different in the case at Venus.

In terms of the space environment, there are three major differences between Venus and Mars. The first is that plasma dynamics on Mars are more kinetic than those on Venus due to the small size of the Martian induced magnetosphere system. Compared with the significant presence of sunward flows at Venus, our results might suggest that kinetic effects (e.g., the finite gyroradius effect) inhibit the generation of these flows. The second is that the plasma density of the Martian ionosphere is far more tenuous than that of the Venusian ionosphere. Thus, solar wind particles could move faster due to a weaker mass-loading effect of the ionosphere. Such a fast tailward plasma convection could inhibit magnetic energy storage and the triggering of magnetic reconnections in the tail. Consequently, the Mars-ward flows triggered by such reconnection would be seldom observed. However, during solar maximum, the ionosphere becomes denser and broader and forms a more Venus-like environment, which could increase the occurrence rate of Mars-ward flows (e.g., Liemohn et al., 2017; Yamauchi et al., 2015). It is expected that the simulations can address the physical links between solar activity and the Mars-ward flows.

The third difference is that Mars possesses localized intense crustal fields, which could organize the plasma dynamics (e.g., Soobiah et al., 2013, 2019; Weber et al., 2021). Here we provide several possible mechanisms. The crustal fields can trap tailward heavy ions, forming the Mars-ward flows that even return to Mars. In addition, non-gyrotropic distribution of ions driven by the crustal fields could sometimes manifest as a Mars-ward flow. For example, when the ions gyrate downward into strong crustal fields, these ions might be nonadiabatic and not move back toward the spacecraft's location when the variable scale of crustal fields is smaller than the gyroradius of particles (e.g., Buchner & Zelenyi, 1986; Soobiah et al., 2019). Furthermore, the ion's energy could also be lost through collision if they move into the deep ionosphere. These may lead to the Mars-ward flows that we observed. This might explain the correlation between crustal fields and Mars-ward flows, as well as there being no dependence on the local elevation angle of crustal fields (since strong ones are below the altitude of spacecraft). However, this mechanism is only valid for Mars-ward flows that occurred at a distance between crustal fields and locations shorter than 2 × gyroradius. It is better to combine the electrons data to further address the physical links between the crustal fields and Mars-ward flow.

For Mars-ward flows that occurred at a high altitude, we suggest that they are a results of tail reconnection and sunward $J \times B$ force (e.g., Gao, Rong, Persson, et al., 2021; Harada et al., 2015a, 2017, 2020; C. Zhang et al., 2022; T. L. Zhang et al., 2012). Therefore, a combination of several mechanisms might drive Mars-ward flows at Mars.

Note that the cold low-energy ions (E/q < 50 eV/q) might be important in studying the Mars-ward flow. For example, the flow that are influence by gravitation (~2 eV for O^+ and 4 eV for O_2^+) is missed in our study, which might explain why the occurrence rate of Mars-ward flows is lower than Venus. In addition, it is meaningless to use the bulk velocity of high-energy ions to identify the Mars-ward flow if the distribution consists of two or

more populations. However, the shape of distribution is hard to determine with the incomplete measurement of low-energy ions. So, we assume that the ions were moving together for all events. Further studies are necessary to address these in the future.

Data Availability Statement

The raw data of ASPERA-3 IMA are available from the Planetary Science Archive (PSA; https://archives.esac.esa.int/psa/ftp/MARS-EXPRESS/ASPERA-3/) and the SPICE kernel repository (https://www.cosmos.esa.int/web/spice/home) at ESA. The method we used to remove the noise contaminations is illustrated in Nilsson et al. (2010, 2011, 2021). The data after noise removal is based on the official pipeline data under development at IRF (Swedish Institute of Space Physics), Kiruna, which will be delivered to Planetary Science Archive (PSA). This effort is based on a contract with the European Space Agency (No. 4000115355). The 13 years of moment data, the selected events, the data for all the figures in this paper are public in the Zenodo repository (https://doi.org/10.5281/zenodo.7233571) (Zhang, 2022). The F10.7 index was retrieved through the OMNI data service at https://omniweb.gsfc.nasa.gov.

Acknowledgments
This work is supported by the National Natural Science Foundation of China (Grants 41922031 and 41774188), the Strategic Priority Research Program of Chinese Academy of Sciences (Grants XDA17010201 and XDB41000000), the Key Research Program of Chinese Academy of Sciences (Grant ZDBS-SSW-TLC00103), the Key Research Program of the Institute of Geology and Geophysics, CAS (Grants IGGCAS- 201904 and IGGCAS-202102), and the European Space Agency (4000115355). C. Zhang is supported by China Scholarship Council (Student 202104910297). C.F. Dong was partially supported by Princeton Plasma Physics Laboratory through the Laboratory Directed Research and Development (LDRD) Program under DOE Prime Contract (DE-AC02-09CH11466). We thank Yuki Harada, Jiawei Gao, Zhen Shi, and Xinzhou Li for their helpful discussion.

References

Barabash, S., Dubinin, E., Pissarenko, N., Lundin, R., & Russell, C. T. (1991). Picked-up protons near Mars: Phobos observations. *Geophysical Research Letters*, *18*(10), 1805–1808. https://doi.org/10.1029/91gl02082

Barabash, S., Fedorov, A., Lundin, R., & Sauvaud, J.-A. (2007). Martian atmospheric erosion rates. *Science*, *315*(5811), 501–503. https://doi.org/10.1126/science.1134358

Barabash, S., Lundin, R., Andersson, H., Brinkfeldt, K., Grigoriev, A., Gunell, H., et al. (2006). The analyzer of space plasma and energetic atoms (ASPERA-3) for the Mars Express Mission. *Space Science Reviews*, *126*, 113. https://doi.org/10.1007/s11214-006-9124-8

Bergman, S., Stenberg Wieser, G., Wieser, M., Johansson, F. L., & Eriksson, A. (2020). The influence of spacecraft charging on low-energy ion measurements made by RPC-ICA on Rosetta. *Journal of Geophysical Research: Space Physics*, *125*(1), e2019JA027478. https://doi.org/10.1029/2019ja027478

Brain, D. A., McFadden, J. P., Halekas, J. S., Connerney, J. E. P., Bougher, S. W., Curry, S., et al. (2015). The spatial distribution of planetary ion fluxes near Mars observed by MAVEN. *Geophysical Research Letters*, *42*(21), 9142–9148. https://doi.org/10.1002/2015gl065293

Buchner, J., & Zelenyi, L. M. (1986). Deterministic chaos in the dynamics of charged particles near a magnetic field reversal. *Physics Letters A*, *118*(8), 395–399. https://doi.org/10.1016/0375-9601(86)90268-9

Collinson, G., Glocer, A., Xu, S., Mitchell, D., Frahm, R. A., Grebowsky, J., et al. (2019). Ionospheric ambipolar electric fields of Mars and Venus: Comparisons between theoretical predictions and direct observations of the electric potential drop. *Geophysical Research Letters*, *46*(3), 1168–1176. https://doi.org/10.1029/2018gl080597

Connerney, J. E. P., Acuña, M. H., Ness, N. F., Kletetschka, G., Mitchell, D. L., Lin, R. P., & Rème, H. (2005). Tectonic implications of Mars crustal magnetism. *Proceedings of the National Academy of Sciences of the United States of America*, *102*(42), 14970–14975. https://doi.org/10.1073/pnas.0507469102

Diéval, C., Stenberg, G., Nilsson, H., & Barabash, S. (2013). A statistical study of proton precipitation onto the Martian upper atmosphere: Mars express observations. *Journal of Geophysical Research: Space Physics*, *118*(5), 1972–1983. https://doi.org/10.1002/jgra.50229

Dong, C., Bougher, S. W., Ma, Y., Lee, Y., Toth, G., Nagy, A. F., et al. (2018). Solar wind interaction with the Martian upper atmosphere: Roles of the cold thermosphere and hot oxygen corona. *Journal of Geophysical Research: Space Physics*, *123*(8), 6639–6654. https://doi.org/10.1029/2018ja025543

Dong, C., Bougher, S. W., Ma, Y., Toth, G., Lee, Y., Nagy, A. F., et al. (2015). Solar wind interaction with the Martian upper atmosphere: Crustal field orientation, solar cycle, and seasonal variations. *Journal of Geophysical Research: Space Physics*, *120*(9), 7857–7872. https://doi.org/10.1002/2015JA020990

Dong, C., Bougher, S. W., Ma, Y., Toth, G., Nagy, A. F., & Najib, D. (2014). Solar wind interaction with Mars upper atmosphere: Results from the one-way coupling between the multifluid MHD model and the MTGCM model. *Geophysical Research Letters*, *41*(8), 2708–2715. https://doi.org/10.1002/2014GL059515

Dong, C., Lee, Y., Ma, Y., Lingam, M., Bougher, S., Luhmann, J., et al. (2018). Modeling Martian atmospheric losses over time: Implications for exoplanetary climate evolution and habitability. *The Astrophysical Journal Letters*, *859*(1), L14. https://doi.org/10.3847/2041-8213/aac489

Dong, Y., Fang, X., Brain, D. A., McFadden, J. P., Halekas, J. S., Connerney, J. E., et al. (2015). Strong plume fluxes at Mars observed by MAVEN: An important planetary ion escape channel. *Geophysical Research Letters*, *42*(21), 8942–8950. https://doi.org/10.1002/2015gl065346

Dong, Y., Fang, X., Brain, D. A., McFadden, J. P., Halekas, J. S., Connerney, J. E. P., et al. (2017). Seasonal variability of Martian ion escape through the plume and tail from MAVEN observations. *Journal of Geophysical Research: Space Physics*, *122*(4), 4009–4022. https://doi.org/10.1002/2016ja023517

Dubinin, E., Fraenz, M., Fedorov, A., Lundin, R., Edberg, N., Duru, F., & Vaisberg, O. (2011). Ion energization and escape on Mars and Venus. *Space Science Reviews*, *162*(1), 173–211. https://doi.org/10.1007/s11214-011-9831-7

Dubinin, E., Fraenz, M., Pätzold, M., Halekas, J. S., Mcfadden, J., Connerney, J. E. P., et al. (2018). Solar wind deflection by mass loading in the Martian magnetosheath based on MAVEN observations. *Geophysical Research Letters*, *45*(6), 2574–2579. https://doi.org/10.1002/2017GL076813

Dubinin, E., Fraenz, M., Pätzold, M., McFadden, J., Mahaffy, P. R., Eparvier, F., et al. (2017). Effects of solar irradiance on the upper ionosphere and oxygen ion escape at Mars: MAVEN observations. *Journal of Geophysical Research: Space Physics*, *122*(7), 7142–7152. https://doi.org/10.1002/2017ja024126

Dubinin, E., Fraenz, M., Woch, J., Zhang, T. L., Wei, J., Fedorov, A., et al. (2012). Bursty escape fluxes in plasma sheets of Mars and Venus. *Geophysical Research Letters*, *39*(1). https://doi.org/10.1029/2011gl049883

Dubinin, E., Fraenz, M., Zhang, T. L., Woch, J., Wei, Y., Fedorov, A., et al. (2013). Plasma in the near Venus tail: Venus express observations. *Journal of Geophysical Research: Space Physics*, *118*(12), 7624–7634. https://doi.org/10.1002/2013ja019164

Fang, X., Liemohn, M. W., Nagy, A. F., Luhmann, J. G., & Ma, Y. (2010). On the effect of the Martian crustal magnetic field on atmospheric erosion. *Icarus*, *206*(1), 130–138. https://doi.org/10.1016/j.icarus.2009.01.012

Fang, X., Liemohn, M. W., Nagy, A. F., Ma, Y., De Zeeuw, D. L., Kozyra, J. U., & Zurbuchen, T. H. (2008). Pickup oxygen ion velocity space and spatial distribution around Mars. *Journal of Geophysical Research*, *113*(A2), A02210. https://doi.org/10.1029/2007ja012736

Fedorov, A., Barabash, S., Sauvaud, J. A., Futaana, Y., Zhang, T. L., Lundin, R., & Ferrier, C. (2011). Measurements of the ion escape rates from Venus for solar minimum. *Journal of Geophysical Research*, *116*(A7), A07220. https://doi.org/10.1029/2011ja016427

Fränz, M., Dubinin, E., Andrews, D., Barabash, S., Nilsson, H., & Fedorov, A. (2015). Cold ion escape from the Martian ionosphere. *Planetary and Space Science*, *119*, 92–102. https://doi.org/10.1016/j.pss.2015.07.012

Fränz, M., Dubinin, E., Roussos, E., Woch, J., Winningham, J. D., Frahm, R., et al. (2006). Plasma moments in the environment of Mars. In *The Mars plasma environment* (pp. 165–207). Springer.

Futaana, Y., Holmström, M., Fedorov, A., & Barabash, S. (2021). Does phobos reflect solar wind protons? Mars express special flyby operations with and without the presence of phobos. *Journal of Geophysical Research: Planets*, *126*(11), e2021JE006969. https://doi.org/10.1029/2021JE006969

Gao, J. W., Rong, Z. J., Klinger, L., Li, X. Z., Liu, D., & Wei, Y. (2021). A spherical harmonic Martian crustal magnetic field model combining data sets of MAVEN and MGS. *Earth and Space Science*, *8*(10), e2021EA001860. https://doi.org/10.1029/2021EA001860

Gao, J. W., Rong, Z. J., Persson, M., Stenberg, G., Zhang, Y. C., Klinger, L., et al. (2021). In situ observations of the ion diffusion region in the Venusian magnetotail. *Journal of Geophysical Research: Space Physics*, *126*(1), e2020JA028547. https://doi.org/10.1029/2020ja028547

Hara, T., Luhmann, J. G., Leblanc, F., Curry, S. M., Halekas, J. S., Seki, K., et al. (2018). Evidence for crustal magnetic field control of ions precipitating into the upper atmosphere of Mars. *Journal of Geophysical Research: Space Physics*, *123*(10), 8572–8586. https://doi.org/10.1029/2017JA024798

Harada, Y., Halekas, J. S., McFadden, J. P., Espley, J., DiBraccio, G. A., Mitchell, D. L., et al. (2017). Survey of magnetic reconnection signatures in the Martian magnetotail with MAVEN. *Journal of Geophysical Research: Space Physics*, *122*(5), 5114–5131. https://doi.org/10.1002/2017ja023952

Harada, Y., Halekas, J. S., McFadden, J. P., Mitchell, D. L., Mazelle, C., Connerney, J. E. P., et al. (2015a). Magnetic reconnection in the near-Mars magnetotail: MAVEN observations. *Geophysical Research Letters*, *42*(21), 8838–8845. https://doi.org/10.1002/2015gl065004

Harada, Y., Halekas, J. S., McFadden, J. P., Mitchell, D. L., Mazelle, C., Connerney, J. E. P., et al. (2015b). Marsward and tailward ions in the near-Mars magnetotail: MAVEN observations. *Geophysical Research Letters*, *42*(21), 8925–8932. https://doi.org/10.1002/2015gl065005

Harada, Y., Halekas, J. S., Xu, S., DiBraccio, G. A., Ruhunusiri, S., Hara, T., et al. (2020). Ion jets within current sheets in the Martian magnetosphere. *Journal of Geophysical Research: Space Physics*, *125*(12), e2020JA028576. https://doi.org/10.1029/2020ja028576

Inui, S., Seki, K., Sakai, S., Brain, D. A., Hara, T., McFadden, J. P., et al. (2019). Statistical study of heavy ion outflows from Mars observed in the Martian-induced magnetotail by MAVEN. *Journal of Geophysical Research: Space Physics*, *124*(7), 5482–5497. https://doi.org/10.1029/2018JA026452

Jakosky, B. M., Brain, D., Chaffin, M., Curry, S., Deighan, J., Grebowsky, J., et al. (2018). Loss of the Martian atmosphere to space: Present-day loss rates determined from MAVEN observations and integrated loss through time. *Icarus*, *315*, 146–157. https://doi.org/10.1016/j.icarus.2018.05.030

Kollmann, P., Brandt, P. C., Collinson, G., Rong, Z. J., Futaana, Y., & Zhang, T. L. (2016). Properties of planetward ion flows in Venus' magnetotail. *Icarus*, *274*, 73–82. https://doi.org/10.1016/j.icarus.2016.02.053

Liemohn, M. W., Xu, S., Dong, C., Bougher, S. W., Johnson, B. C., Ilie, R., & De Zeeuw, D. L. (2017). Ionospheric control of the dawn-dusk asymmetry of the Mars magnetotail current sheet. *Journal of Geophysical Research: Space Physics*, *122*(6), 6397–6414. https://doi.org/10.1002/2016ja023707

Luhmann, J. G., Ledvina, S. A., & Russell, C. T. (2004). Induced magnetospheres. *Advances in Space Research*, *33*(11), 1905–1912. https://doi.org/10.1016/j.asr.2003.03.031

Lundin, R. (2011). Ion acceleration and outflow from Mars and Venus: An overview. *The Plasma Environment of Venus, Mars, and Titan*, *162*(1–4), 309–334. https://doi.org/10.1007/s11214-011-9811-y

Lundin, R., Zakharov, A., Pellinen, R., Borg, H., Hultqvist, B., Pissarenko, N., et al. (1989). First measurements of the ionospheric plasma escape from Mars. *Nature*, *341*(6243), 609–612. https://doi.org/10.1038/341609a0

Ma, Y., Nagy, A. F., Hansen, K. C., DeZeeuw, D. L., Gombosi, T. I., & Powell, K. (2002). Three-dimensional multispecies MHD studies of the solar wind interaction with Mars in the presence of crustal fields. *Journal of Geophysical Research*, *107*(A10), 1282–1289. https://doi.org/10.1029/2002ja009293

Ma, Y. J., Dong, C. F., Toth, G., van der Holst, B., Nagy, A. F., Russell, C. T., et al. (2019). Importance of ambipolar electric field in driving ion loss from Mars: Results from a multifluid MHD model with the electron pressure equation included. *Journal of Geophysical Research: Space Physics*, *124*(11), 9040–9057. https://doi.org/10.1029/2019ja027091

Masunaga, K., Futaana, Y., Persson, M., Barabash, S., Zhang, T. L., Rong, Z. J., & Fedorov, A. (2019). Effects of the solar wind and the solar EUV flux on O^+ escape rates from Venus. *Icarus*, *321*, 379–387. https://doi.org/10.1016/j.icarus.2018.11.017

Nilsson, H., Carlsson, E., Brain, D. A., Yamauchi, M., Holmström, M., Barabash, S., et al. (2010). Ion escape from Mars as a function of solar wind conditions: A statistical study. *Icarus*, *206*(1), 40–49. https://doi.org/10.1016/j.icarus.2009.03.006

Nilsson, H., Edberg, N. J. T., Stenberg, G., Barabash, S., Holmström, M., Futaana, Y., et al. (2011). Heavy ion escape from Mars, influence from solar wind conditions and crustal magnetic fields. *Icarus*, *215*(2), 475–484. https://doi.org/10.1016/j.icarus.2011.08.003

Nilsson, H., Stenberg, G., Futaana, Y., Holmström, M., Barabash, S., Lundin, R., et al. (2012). Ion distributions in the vicinity of Mars: Signatures of heating and acceleration processes. *Earth Planets and Space*, *64*(2), 135–148. https://doi.org/10.5047/eps.2011.04.011

Nilsson, H., Zhang, Q., Wieser, G. S., Holmström, M., Barabash, S., Futaana, Y., et al. (2021). Solar cycle variation of ion escape from Mars. *Icarus*, 114610. https://doi.org/10.1016/j.icarus.2021.114610

Persson, M., Futaana, Y., Fedorov, A., Nilsson, H., Hamrin, M., & Barabash, S. (2018). H^+/O^+ escape rate ratio in the Venus magnetotail and its dependence on the solar cycle. *Geophysical Research Letters*, *45*(20), 10–805. https://doi.org/10.1029/2018gl079454

Persson, M., Futaana, Y., Ramstad, R., Masunaga, K., Nilsson, H., Hamrin, M., et al. (2020). The Venusian atmospheric oxygen ion escape: Extrapolation to the early solar system. *Journal of Geophysical Research: Planets*, *125*(3), e2019JE006336. https://doi.org/10.1029/2019je006336

Ramstad, R., Barabash, S., Futaana, Y., Nilsson, H., & Holmström, M. (2016). Effects of the crustal magnetic fields on the Martian atmospheric ion escape rate. *Geophysical Research Letters*, *43*(20), 10574–10579. https://doi.org/10.1002/2016GL070135

Ramstad, R., Barabash, S., Futaana, Y., Nilsson, H., & Holmström, M. (2018). Ion escape from Mars through time: An extrapolation of atmospheric loss based on 10 years of Mars express measurements. *Journal of Geophysical Research: Planets*, *123*(11), 3051–3060. https://doi.org/10.1029/2018je005727

Ramstad, R., Barabash, S., Futaana, Y., Nilsson, H., Wang, X. D., & Holmström, M. (2015). The Martian atmospheric ion escape rate dependence on solar wind and solar EUV conditions: 1. Seven years of Mars express observations. *Journal of Geophysical Research: Planets*, *120*(7), 1298–1309. https://doi.org/10.1002/2015je004816

Rojas-Castillo, D., Nilsson, H., & Stenberg Wieser, G. (2018). Mass composition of the escaping flux at Mars: MEX observations. *Journal of Geophysical Research: Space Physics*, *123*(10), 8806–8822. https://doi.org/10.1029/2018ja025423

Soobiah, Y. I. J., Barabash, S., Nilsson, H., Stenberg, G., Lundin, R., Coates, A. J., et al. (2013). Energy distribution asymmetry of electron precipitation signatures at Mars. *Planetary and Space Science*, *76*, 10–27. https://doi.org/10.1016/j.pss.2012.10.014

Soobiah, Y. I. J., Espley, J. R., Connerney, J. E. P., Gruesbeck, J. R., DiBraccio, G. A., Halekas, J., et al. (2019). MAVEN case studies of plasma dynamics in low-altitude crustal magnetic field at Mars 1: Dayside ion spikes associated with radial crustal magnetic fields. *Journal of Geophysical Research: Space Physics*, *124*(2), 1239–1261. https://doi.org/10.1029/2018JA025569

Trotignon, J. G., Mazelle, C., Bertucci, C., & Acuña, M. H. (2006). Martian shock and magnetic pile-up boundary positions and shapes determined from the Phobos 2 and Mars Global Surveyor data sets. *Planetary and Space Science*, *54*(4), 357–369. https://doi.org/10.1016/j.pss.2006.01.003

Voshchepynets, A., Barabash, S., Ramstad, R., Holmstrom, M., Andrews, D., Nicolaou, G., et al. (2018). Ions accelerated by sounder-plasma interaction as observed by Mars express. *Journal of Geophysical Research: Space Physics*, *123*(11), 9802–9814. https://doi.org/10.1029/2018ja025889

Weber, T., Brain, D., Xu, S., Mitchell, D., Espley, J., Mazelle, C., et al. (2021). Martian crustal field influence on O^+ and O_2^+ escape as measured by MAVEN. *Journal of Geophysical Research: Space Physics*, *126*(8), e2021JA029234. https://doi.org/10.1029/2021JA029234

Xu, S., Mitchell, D. L., Ma, Y., Weber, T., Brain, D. A., Halekas, J., et al. (2021). Global ambipolar potentials and electric fields at Mars inferred from MAVEN observations. *Journal of Geophysical Research: Space Physics*, *126*(12), e2021JA029764. https://doi.org/10.1029/2021ja029764

Yamauchi, M., Hara, T., Lundin, R., Dubinin, E., Fedorov, A., Sauvaud, J. A., et al. (2015). Seasonal variation of Martian pick-up ions: Evidence of breathing exosphere. *Planetary and Space Science*, *119*, 54–61. https://doi.org/10.1016/j.pss.2015.09.013

Zhang, C. (2022). Supporting data for Mars-ward ion flows in the Martian magnetotail: Mars express observations [Dataset]. Zenodo. https://doi.org/10.5281/zenodo.7233571

Zhang, C., Rong, Z., Klinger, L., Nilsson, H., Shi, Z., He, F., et al. (2022). Three-dimensional configuration of induced magnetic fields around Mars. *Journal of Geophysical Research: Planets*, *127*(8), e2022JE007334. https://doi.org/10.1029/2022JE007334

Zhang, C., Rong, Z., Nilsson, H., Klinger, L., Xu, S., Futaana, Y., et al. (2021). MAVEN observations of periodic low-altitude plasma clouds at Mars. *The Astrophysical Journal Letters*, *922*(2), L33. https://doi.org/10.3847/2041-8213/ac3a7d

Zhang, T. L., Lu, Q. M., Baumjohann, W., Russell, C. T., Fedorov, A., Barabash, S., et al. (2012). Magnetic reconnection in the near Venusian magnetotail. *Science*, *336*(6081), 567–570. https://doi.org/10.1126/science.1217013